Available online at www.sciencedirect.com
SCIENCE DIRECT®
European Journal of Mechanics B/Fluids 24 (2005) 457–467

Simulation of the rarefied gas flow around a perpendicular disk

A. Chpoun [a,b], T.G. Elizarova [c], I.A. Graur [d], J.C. Lengrand [a,*]

[a] *Lab. d'Aérothermique, CNRS, 1C, av. de la recherche scientifique, 45071 Orléans cedex 2, France*
[b] *LMEE, Université d'Evry, rue Pelvoux, 91000 Evry, France*
[c] *Instit. for Mathematical Modelling, Russian Acad. of Science, Miusskaya sq. 4a, 125047 Moscow, Russia*
[d] *Polytech'Marseille, IUSTI, 5 r. Enrico Fermi, 13453 Marseille cedex 13, France*

Received 17 November 2003; received in revised form 4 May 2004; accepted 30 October 2004

Available online 5 March 2005

Abstract

The present work contributes to define the domain of validity of two continuum approaches, based on Navier–Stokes (NS) and quasi gas-dynamic (QGD) equations, respectively. Results obtained using each method are compared with those obtained using a direct simulation Monte Carlo (DSMC) method considered as a reference. QGD equations differ from NS ones by the presence of additional dissipative terms. The present paper includes a brief presentation of QGD equations and DSMC procedures used here. The rarefied flow around a perpendicular disk has been considered for a freestream Mach number varying from 2 to 20, a Knudsen number equal to 0.1 and two levels of wall temperature.
© 2004 Elsevier SAS. All rights reserved.

Keywords: Rarefied gas dynamics; Disk; Continuum equations; Monte Carlo simulation

1. Introduction

The interest of defining the domain of validity of continuum approaches for rarefied gas flows is due to the fact that solving continuum equations requires usually less computational resources than using methods based on a molecular description, such as Bird's Direct Simulation Monte Carlo (DSMC) method [1]. This is a particular advantage for the simulation of non-stationary flows. In addition to the Navier–Stokes (NS) equations, another set of continuum equations, namely the quasi gas-dynamic (QGD) equations, are considered [2]. They can be regarded as a promising approach for the description of viscous gas flows, but the domain of validity of these equations has not been sufficiently investigated. Data obtained by DSMC are used as a reference. The physical modeling is made consistent in all calculations, but DSMC results are free from the near-equilibrium hypothesis that is included in the continuum approaches.

The domain of validity of continuum NS and QGD approaches compared with the DSMC model was investigated in [3] for the flow along a semi-infinite sharp flat plate. It was found, that QGD equations bring an improvement compared with NS ones in the vicinity of the leading edge. Otherwise QGD and NS results tend to coincide one with another and with the DSMC data. For a given numerical procedure, QGD equations are more stable than NS ones. For rather large Knudsen numbers, the advantage of the QGD model compared with the NS one in estimating the mass-flow rate in a plane micro-channel was

* Corresponding author.
E-mail addresses: chpoun@iut.univ-evry.fr (A. Chpoun), telizar@yahoo.com (T.G. Elizarova), Irina.Graour@polytech.univ-mrs.fr (I.A. Graur), lengrand@cnrs-orleans.fr (J.C. Lengrand).

0997-7546/$ – see front matter © 2004 Elsevier SAS. All rights reserved.
doi:10.1016/j.euromechflu.2004.10.007

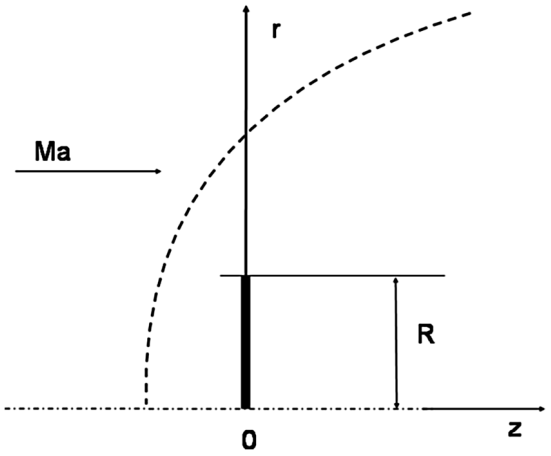

Fig. 1. Definition of the problem.

demonstrated in [4]. Experimental data were used as a reference. The application of QGD equations to the underexpanded jet problem [5,6] and their generalization to binary gas mixtures [7] illustrate other possibilities of this approach.

In addition to the above-mentioned problems we consider now an infinitely thin circular disk perpendicular to a supersonic freestream (Fig. 1). The problem is difficult from a computational point of view due to strong gradients and large differences in the density levels encountered ahead of a disk and in the near wake. A similar problem (70 degrees blunted cone) had been retained as a test-case studied both experimentally and numerically by a number of workers, with particular interest for the wake region [8], and for the heat transfer rate, with potential applications to future Mars entry missions [9].

In this paper we present a comparison of NS, QGD and DSMC approaches for the flow around a disk, with emphasis on wall quantities (skin-friction, pressure and heat-flux distributions on the forward-facing disk surface), as well as on density, temperature and velocity distributions in the near-wake region. A systematic study has been carried out for a freestream Mach number Ma_∞ equal to 2, 5 and 20 and for a wall temperature T_w equal to the freestream stagnation temperature T_0 and to $0.5T_0$, successively. The Knudsen number $Kn = \lambda_\infty/(2R)$ was equal to 0.1, where λ_∞ denotes the mean free path and R the radius of the disk. The subscript $()_\infty$ refers to freestream conditions and will be dropped when there will be no ambiguity. The cases $Kn = 0.01$ and 0.005 have been also considered but will not be discussed here. Particular attention has been paid to using consistent physical modeling in all approaches considered: monoatomic hard-sphere gas with full accommodation at the wall, resulting in a viscosity law $\mu \propto T^{0.5}$ and a Prandtl number Pr equal to $2/3$.

2. Gas dynamic equations and boundary conditions

Gas-dynamic equations consist of a system of three partial-derivative equations

$$\frac{\partial \rho}{\partial t} + \nabla_i J^i = 0 \quad \text{(conservation of mass)}, \tag{1}$$

$$\frac{\partial (\rho u^k)}{\partial t} + \nabla_i J^i u^k + \nabla^k p = \nabla_i \Pi^{ik} \quad \text{(conservation of momentum)}, \tag{2}$$

$$\frac{\partial E}{\partial t} + \nabla_i \frac{J^i}{\rho}(E + p) + \nabla_i q^i = \nabla_i (\Pi^{ik} u^k) \quad \text{(conservation of energy)}, \tag{3}$$

with $E = 0.5\rho u^i u_i + \rho\varepsilon$. Here ρ is the density, $\vec{u}$ the velocity-vector, $p = \rho\mathcal{R}T/\mathcal{M}$ the pressure, $\mathcal{M}$ the molar mass, $\mathcal{R}$ the perfect-gas constant, T the temperature, $\varepsilon = p/(\rho(\gamma - 1))$ the internal energy, γ the specific heat ratio. To close the system (1)–(3), the mass flux vector J^i, the shear-stress tensor Π^{ik}, and the heat flux vector q^i must be expressed as a function of macroscopic flow quantities. Different expressions for these quantities lead either to the NS equations, or to the QGD equations.

NS equations are based on

$$J^i = J^i_{\mathrm{NS}} = \rho u^i, \tag{4}$$

$$\Pi^{ik} = \Pi^{ik}_{\mathrm{NS}} = \mu\big[\nabla^k u^i + \nabla^i u^k - (2/3) g^{ik} \nabla_j u^j\big], \tag{5}$$

$$q^i = q^i_{\mathrm{NS}} = -\kappa \nabla^i T. \tag{6}$$

Here g^{ik} is the metric tensor, μ and κ are the viscosity and heat conductivity coefficients, respectively. According to [2], the system (1)–(3) can be closed also by

$$J^i = J^i_{\mathrm{NS}} - \tau\big(\nabla_j(\rho u^i u^j) + \nabla^i p\big), \tag{7}$$

$$\Pi^{ik} = \Pi^{ik}_{\mathrm{NS}} + \tau u^i(\rho u^j \nabla_j u^k + \nabla^k p) + \tau g^{ik}(u_j \nabla^j p + \gamma p \nabla_j u^j), \tag{8}$$

$$q^i = q^i_{\mathrm{NS}} - \tau\rho u^i\left(u^j\nabla_j\varepsilon + p u_j \nabla^j\left(\frac{1}{\rho}\right)\right). \tag{9}$$

Here the parameter τ is Maxwell's relaxation time, equal to μ/p and close to the mean time between successive molecular collisions. This expression of τ is consistent with another derivation of QGD equations, based on a kinetic model (Boltzmann equation in BGK approximation supplemented with an approximation of the distribution function in the Taylor decomposition form, e.g. [3,7]).

The conservation of mass, momentum, total energy and the entropy theorem are valid for QGD equations as for the classical NS ones. QGD and NS systems differ by terms of $\mathrm{O}(\tau)$, or in dimensionless form, by terms of $\mathrm{O}(Kn)$ when $Kn \to 0$. For stationary flows, the difference is of $\mathrm{O}(Kn^2)$. These additional dissipative terms in the QGD system work as a stabilizer of the numerical scheme for the NS system. However, QGD system is non-Galilean invariant, and the non-Galilean invariance comes from these additional terms of $\mathrm{O}(Kn^2)$. The latter are space-derivatives of the second order and they differ from the Burnett additional terms that are space derivatives of the third order. A review of theoretical and numerical results for QGD equations can be found in [2].

The problem definition scheme is shown in Fig. 1. The radial and axial components of the velocity vector were denoted u_r and u_z, respectively. The conditions at the left (upstream) boundary are those in the undisturbed flow: $u_z = V_\infty$, $u_r = 0$, $p = p_\infty$, $\rho = \rho_\infty$. At the right (downstream) and upper (lateral) boundaries, so-called "soft" conditions are prescribed: $\partial f/\partial n = 0$ where $f = (u_r, u_z, p)$ for NS and $f = (\rho, u_r, u_z, p)$ for QGD. n is the co-ordinate normal to the boundary. Symmetry conditions are applied on the axis. At the disk surface, conditions for velocity slip and temperature jump are prescribed

$$u_s = \left(\frac{\mu}{\rho}\sqrt{\frac{\pi\mathcal{M}}{2\mathcal{R}T}}\frac{\partial u_t}{\partial n}\right)_s \quad \text{and} \quad T_s - T_w = \left(\frac{\kappa\mathcal{M}}{2\rho\mathcal{R}}\sqrt{\frac{\pi\mathcal{M}}{2\mathcal{R}T}}\frac{\partial T}{\partial n}\right)_s, \tag{10}$$

where u_t is the tangential velocity and the subscript s refers to the gas parameters along the wall. These boundary conditions were complemented by the no-flow condition $u_n = 0$ and by the additional pressure condition $\partial p/\partial n = 0$ for the QGD system. The last two conditions ensure the absence of mass flux across the boundary $J^i = J^i_{\mathrm{NS}} = 0$. The no-flow velocity condition leads to identical expressions of momentum, heat flux and energy exchange in QGD and NS equations on the solid wall:

$$\Pi^{ik} = \Pi^{ik}_{\mathrm{NS}} = \sigma = \mu\frac{\partial u_t}{\partial n}, \quad q^i = q^i_{\mathrm{NS}} = \kappa\frac{\partial T}{\partial n}, \quad q_E = \mu u_t\frac{\partial u_t}{\partial n} + \kappa\frac{\partial T}{\partial n}.$$

3. Flow conditions

It was supposed (rather arbitrarily) that the working gas was Argon, characterized by a specific heat ratio $\gamma = 5/3$ (monoatomic). Considered as a hard-sphere gas, with a molecular diameter equal to $d = 3.622 \times 10^{-10}$ m, and a molecular mass $m = 6.634 \times 10^{-26}$ kg m^{-3}, its viscosity is given by Bird [1] as

$$\mu = \frac{5}{16d^2}\sqrt{\frac{mkT}{\pi}}, \quad \text{where } k \text{ is the Boltzmann constant.} \tag{11}$$

The freestream temperature T_∞ and number density n_∞ were taken equal to 273 K and 1.716×10^{18} molecules m^{-3}, respectively, resulting in a collision frequency $\nu = 4nd^2\sqrt{kT\pi/m} = 380.4$ s^{-1} and a mean free path $\lambda_\infty = 1$ m.

A number of parameters relative to the different flow conditions considered is presented in Table 1. It includes quantities $\rho_\infty V_\infty^2$ and $\rho_\infty V_\infty C_p(T_0 - T_w)$. The first one is used to normalize the wall skin-friction and get the skin-friction coefficient $C_f/2 = \sigma/(\rho_\infty V_\infty^2)$ whereas the second one is used to normalize the wall heat transfer in the case $T_w = 0.5T_0$ and get the heat transfer coefficient (Stanton number) $C_h = q_E/(\rho_\infty V_\infty C_p(T_0 - T_w))$. In the near-adiabatic case ($T_w = T_0$), the thermal flux was not considered.

Stagnation parameters p_0 and T_0 are defined as

$$p_0 = p_\infty\left(1 + \frac{\gamma-1}{2}Ma_\infty^2\right)^{\gamma/(\gamma-1)}, \qquad T_0 = T_\infty\left(1 + \frac{\gamma-1}{2}Ma_\infty^2\right).$$

Table 1
Flow parameters

Mach number Ma_∞	2	5	10	20
Stagnation temperature T_0 (K)	637.0	2548	9373	36673
Velocity V_∞ (m/s)	615.5	1538.7	3077	6155
Reynolds number $Re = 2\rho_\infty V_\infty R/\mu_\infty$	32.96	82.40	164.81	329.6
Reduced stagnation pressure p_{i2}/p_∞	6.345	37.17	147.3	588.0
$\rho_\infty V_\infty^2$ (Pa)	0.04311	0.26944	1.07775	4.31099
Information for $T_w = T_0$:				
Wall temperature ratio T_w/T_∞	2.333	9.333	34.33	134.3
p_{fm}/p_∞ on forward-facing side	12.61	67.38	262.5	1043
Information for $T_w = T_0/2$:				
Wall temperature ratio T_w/T_∞	1.167	4.667	17.16	67.15
$\rho_\infty V_\infty C_p(T_0 - T_w)$ (W/m^2)	11.61	116.1	854.0	6683
p_{fm}/p_∞ on forward-facing side	11.16	60.14	234.7	932.9

Table 2
Characteristic parameters of DSMC runs

Run	Near-adiabatic case $T_w = T_0$						Cold-wall case $T_w = T_0/2$			
	*E*1	*A*4	*B*2	*D*2	*A*5	*A*8	*E*3	*A*10	*A*12	*A*13
Ma_∞	2	5	5	5	5	20	2	5	20	20
Grid	E	A	B	D	A	A	E	A	A	A
δt (ms)	0.5	0.2	0.2	0.2	0.1	0.05	0.45	0.15	0.025	0.01
t_{stat} (s)	0.25	0.1	0.1	0.1	0.1	0.02	0.2	0.05	0.03	0.03
t_{final} (s)	1.24	0.36	0.43	0.25	0.48	0.134	3.25	0.59	0.24	0.088
$v\delta t <$	0.8	0.94	0.93	0.95	0.46	0.96	0.95	0.9	0.64	0.26
$V_\infty \delta t$ (m)	0.31	0.31	0.31	0.31	0.15	0.31	0.28	0.23	0.153	0.062

4. DSMC calculations

Direct Simulation Monte Carlo (DSMC) calculations were carried out using the code DISIRAF (DIrect SImulation of RArefied Flows) developed at the Laboratoire d'Aérothermique du CNRS, based on the ideas of Bird [1]. This code has already been applied to a variety of problems, e.g. [3,9]. The molecular interaction was described by the VHS (Variable Hard Sphere) model used here in the particular case of hard-spheres molecules. Consistency with NS and QGD calculations was ensured by the relation (11) between viscosity and reference collisional cross-section. The correct molecular frequency was ensured by using the NTC (No Time Counter) algorithm.

The number of real molecules simulated by a computational molecule was variable. In a given cell, it was taken equal to $(n_{\text{approx}} V_{\text{cell}})/10$, where n_{approx} was an estimation of the local number density and V_{cell} the volume of the cell. This would ensure a uniform cell population of $N_c = 10$ computational molecules if n were exact. For an initial calculation, n_{approx} was taken equal to n_∞. This resulted in a cell population that ranged from less than one molecule to tens of molecules. The number density resulting from the initial solution was then used as a better estimate of n. The weighting factor of the molecules was readjusted and a new calculation was launched. The number of computational molecules per cell was found rather uniform and the results were retained.

Molecules were injected through the upstream ($z = z_{\min} = -13$ m) and lateral boundaries with distribution functions corresponding to freestream conditions. The disk ($z = 0$, $0 < r < r_{\max}$) was considered as a diffusely reflecting surface with perfect accommodation at wall temperature T_w. The inward flow-rate of molecules through the downstream boundary ($z = z_{\max}$) was neglected because of the supersonic nature of the flow. A fraction of the computational time was used to reach the steady state ($0 < t < t_{\text{stat}}$). Then the computation was continued ($t_{\text{stat}} < t < t_{\text{final}}$) to gather statistical information by sampling the flowfield and recording exchanges between the gas and the wall. The values of t_{stat} and t_{final}, as well as a number of other data are given in Table 2 for the different runs.

Different grids were used to check the sensitivity of the results to the grid parameters, and to the extent of the computational domain. The scheme of the grids is shown in Fig. 2. The intersection of the grid with the disk plane was used to divide both faces of the disk into N_3 surface elements. The minimal cell size is imposed near the $z = 0$ plane (z-direction) and near the disk edge (in the r-direction). Space steps δz and δr changed by a constant factor f between adjacent cells. The meaning of subscripts 1,

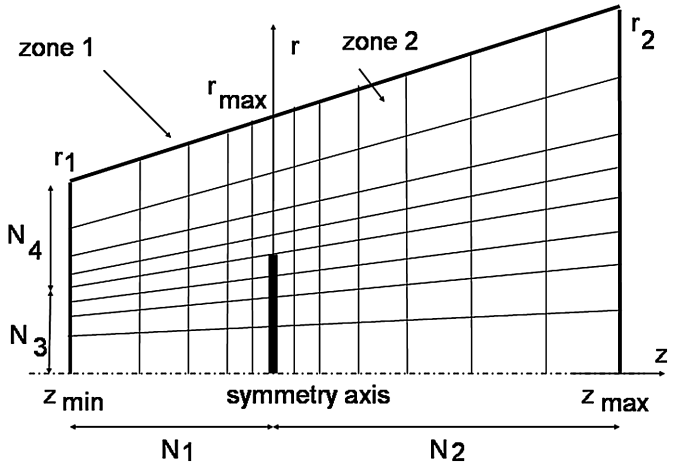

Fig. 2. Scheme of computational domain.

2, 3, 4 is made clear in Fig. 2. The number of cells in grids A, B, D and E was 4875, 4736, 1320 and 4875, respectively. The values of (N_1, N_2, N_3, N_4) were (30, 45, 30, 35) for grids A and D, (30, 44, 30, 34) for grid B, (16, 24, 15, 18) for grid C.

It is generally admitted that the cell size must be small compared with both the gradient length scale and the local mean free path. The first condition is required to ensure a correct space resolution. The second condition is based on the fact that collision partners are chosen within the same cell, irrespective of their actual position. Thus the cell should have dimensions smaller than a mean free path to prevent unrealistic collisions to take place. In fact, when the first condition is satisfied, collision partners are sampled with the correct distribution functions, even when they are more than one mean free path apart. Thus only the first condition is necessary, but it may be as severe as the second one in some regions (shock wave structure, Knudsen layer, etc.) where the gradient length scale is governed by the local mean free path. Thus the cell size in any direction $\vec{x}$ must be such that $|\delta\vec{x} \cdot \vec{\nabla} Q/Q| \ll 1$, where Q is the most rapidly changing flow parameter.

It is also generally admitted that the time step δt must be sufficiently small to ensure that the following condition holds in each cell

$$\nu\delta t < 1 \quad \text{or} \quad \delta t < 1/\nu = \tau_c \quad \text{(mean time between collisions)}. \tag{12}$$

This condition is due to uncoupling the processes of moving and colliding molecules with time step δt. An additional condition is due to the fact that computational collisions take place at the end of the molecular moving rather than at any time during time interval δt. The collisional partners of a given molecule are representative of the real ones only if the macroscopic parameters of the flow do not change significantly along the path traveled by the molecule during δt. This condition has different expressions in a supersonic flow (molecular displacement is governed essentially by the macroscopic flow velocity $\vec{u}$) and in a subsonic flow (it is governed essentially by the thermal speed c)

$$\delta t < \frac{|Q|}{|\vec{u} \cdot \vec{\nabla} Q|} \quad \text{(locally supersonic)}, \tag{13}$$

$$\delta t < \frac{|Q|}{\bar{c} \times |\vec{\nabla} Q|} = \frac{\tau_c}{\lambda} \times \frac{|Q|}{|\vec{\nabla} Q|} \quad \text{(locally subsonic)}. \tag{14}$$

In a subsonic flow, the gradient length scale $|Q|/|\vec{\nabla} Q|$ cannot be smaller than the mean free path λ and condition (14) is not more severe than condition (12). In a supersonic flow, condition (13) is often overlooked, although it may be more severe than the usual condition (12) by a factor approximately equal to the Mach number. To give an indication of how condition (13) is satisfied, the product $V_\infty \delta t$ is given in Table 2. This quantity is to be compared with the gradient length scales ($\approx R = 5$ meters when governed by the geometry).

A reference calculation $A4$ was run with grid A and $\delta t = 2 \times 10^{-4}$ s for $Ma_\infty = 5$, $T_w = T_0$. The same case ($B2$) was recalculated with the same parameters using grid B which differs only by the absence of the last downstream row of cells. Then grid D was used (run $D2$). It was characterized by cell dimensions larger by a factor of 2 in both directions. Finally calculation $A5$ was run with a time step smaller by a factor of 2, ensuring $\nu\delta t < 0.46$ in any cells, whereas the other calculations resulted in $\nu\delta t < 0.95$. It was found that displacing the downstream boundary or using a smaller time step does not change the results. Using the coarse grid D affects slightly the shock structure but has no visible influence on the other quantities.

To check for the possible influence of time step in a high supersonic conditions, calculation $A12$ was run with grid A and $\delta t = 2.5 \times 10^{-5}$ s for $Ma_\infty = 20$, $T_w = T_0/2$. The same case was recalculated as run $A13$ with the same parameters except that the time step was equal to 10^{-5} s. All results of run $A13$ coincide with those of run $A12$ within statistical scatter.

Thus the DSMC results presented in the present work can be considered as free from discretization errors. The runs whose results have been used for comparison with QGD and NS ones are underlined in Table 2.

5. NS calculations

The numerical results were obtained using the finite volume zonal commercial code INCA [10]. In short, the code solves the complete Navier–Stokes equations by means of a time marching method. The evaluation of the inviscid terms are based on flux splitting in combination with upwind based differencing. The code supports the flux-vector-splitting method of Steger and Warming. The diffusion terms are evaluated using standard central differences. The LU-SGS algorithm is used to solve the system using Gauss–Seidel relaxation. Viscosities are evaluated using a power law $\mu \propto T^{1/2}$ consistent with both DSMC and QGD methods. The computational domain is divided into two zones shown in Fig. 2. It contains (30×100) cells in zone 1 and (70×100) cells in zone 2. The grid structure is very similar to the DSMC grid that has been described in Section 4.

An infinitely thin surface was considered to separate the two zones. The computational domain was large enough for freestream conditions to be specified at the upstream and lateral boundaries. Downstream outflow quantities were extrapolated.

The sensitivity of numerical results to mesh refinement was analyzed for $Ma = 20$ and $T_w = T_0/2$. Results were obtained for two different grids (100×100 and 100×60). The smallest cells near the disk edge had $(z \times r)$ dimensions equal to $(0.01R \times 0.02R)$ and $(0.02R \times 0.04R)$ respectively. The results obtained for the distributions of adimensional pressure and z-component of velocity along the symmetry axis at the same convergency level are very close to one another. Thus NS results can be regarded as free from discretization errors.

6. QGD calculations

For the numerical calculations an explicit in time finite-volume method was used, similar to that described in [5]. The axisymmetric form of QGD equations (1)–(3), (7)–(9) was used in a non-dimensional form with $\mu = \tau p$. The corresponding scaling quantities are taken in the freestream region: mean free path λ_∞, density ρ_∞, sound velocity $a_\infty = \sqrt{\gamma RT_\infty}$, temperature T_∞.

The rectangular computational domain is covered with a rectangular non-uniform grid with steps δ_r and δ_z. The smallest space steps in the r-direction are situated near the disk edge ($\delta_r = 0.2$) and near the axis. The smallest space steps ($\delta_z = 0.2$) in the z-direction are placed near the disk plane. Between adjacent cells, δ_r and δ_z increase by constant factors. The position of the upper boundary $r_{\max}$ is taken sufficiently large for the upper boundary to be located entirely in the undisturbed freestream. The symmetry axis and the disk surface are placed half-way between the nodes. The thickness of the disk is equal to δ_z.

An explicit finite-difference scheme is constructed. Space derivatives are approximated by a centered scheme. Flow parameters are calculated in the nodes of the computational grid. Quantities at the centered points between the nodes are calculated as the average of the quantities at the two nearest nodes. Mixed derivatives are calculated as $1/4$ of the sum of the corresponding quantities in the nearest four points. Time derivatives are approximated with first accuracy order. Freestream conditions are used as inflow and initial conditions. Boundary conditions (10) are treated as algebraic equations whose coefficients are taken from the previous time step. At the disk surface, μ_s is calculated as $\mu_s = \mu(T_s)$.

When solving QGD equations, oscillations appeared for $Ma_\infty = 20$ in regions with strong gradients. To overcome the problem μ was replaced by $\mu + \mu'$, where $\mu' = \beta p \delta / a$ in the dissipative terms, except in those with mixed spatial derivatives. δ is the local space step, a is the speed of sound, β is the smallest possible damping parameter that ensures the stability of the solution. The same procedure was used successfully in a number of supersonic calculations, e.g. [3,5]. For $Ma_\infty = 20$, β was taken equal to 0.1. For all other cases, there was no need to stabilize the solution. The steady-state solution is obtained as the limit of a time-evolving process. The computation stops when the steady-state solution is reached. The time step is based on the Courant stability condition $\delta t = \alpha \min(\delta / V)$, where $V = a + \sqrt{u_r^2 + u_z^2}$. The coefficient α is chosen empirically and ranges from 0.005 to 0.02.

Grid dependence of the results was studied by repeating a calculations for $Ma_\infty = 5$ with space steps twice smaller in both directions. Distributions of flow parameters and wall quantities obtained with grids 78×74 and 155×147 are very close to one another or indistinguishable. To check for the influence of the stabilizing parameter β, the test case $Ma_\infty = 2$ was calculated for $\beta = 0$ and $\beta = 0.1$. Increasing β smooths slightly the pressure and density gradients in the expansion fan, which results in a small increase of pressure and density in the wake of the disk. The rest of the flowfield is not influenced by β. Thus the present QGD results are not significantly affected by finite discretization nor by the introduction of the stabilizing parameter β.

7. Results and discussion

The distributions of wall and flow quantities obtained by all three methods have been plotted together and will be commented upon in this section. Freestream quantities are used to make all plotted results dimensionless.

Wall quantities are of interest for practical applications. The pressure p and the shear stress σ are plotted in a dimensionless form (p/p_∞, $C_f/2 = \sigma/(\rho_\infty V_\infty^2)$) in the left part of Fig. 3 for the flow conditions $Ma_\infty = 2$, 5 and 20, $T_w = T_0$. DSMC makes a difference between normal stress F_n due to molecular normal momentum exchange and pressure p deduced from the equation-of-state near the wall. Near the disk edge, results may be affected by details of the treatment for the singularity. All pressure results are close to one another. The reduced pressure on the forward-facing side is close to the reduced Newtonian approximation p_{i2}/p_∞ while the free-molecular estimation (p_{fm}/p_∞) would be approximately twice larger (see Table 1). For $Ma_\infty = 20$ and even for $Ma_\infty = 5$, the skin-friction coefficient is much better predicted by QGD than by NS equations. For $Ma_\infty = 2$, the flow is closer to equilibrium and all methods give similar results.

For the cold-wall problem ($T_w = T_0/2$, $Ma = 2$ and 20), the distributions of $C_f/2$ and C_h are plotted in the right part of Fig. 3. QGD equations result again in a better estimation of $C_f/2$. The differences between NS and QGD results increase with increasing the Mach number. The heat transfer rates obtained by the three methods are close to one another.

The axial distributions of ρ, T and axial velocities for $Ma_\infty = 5$, $T_w = T_0$ are shown in Fig. 4. The disk is located in the plane $z = 0$. QGD velocities are presented in two forms – as u and as $u^J = J/\rho$, based on the mass flux J given by Eq. (7). The difference between these velocities is proportional to τ and goes to zero for small local Knudsen numbers. The density and both velocity profiles along the stagnation line are nearly insensitive to the model. The main differences are seen for the temperature profiles ahead of the shock. The QGD temperature profile departs from the freestream value earlier than NS and DSMC profiles. Compared with DSMC results, NS and QGD results exhibit differences in opposite directions. The main differences between

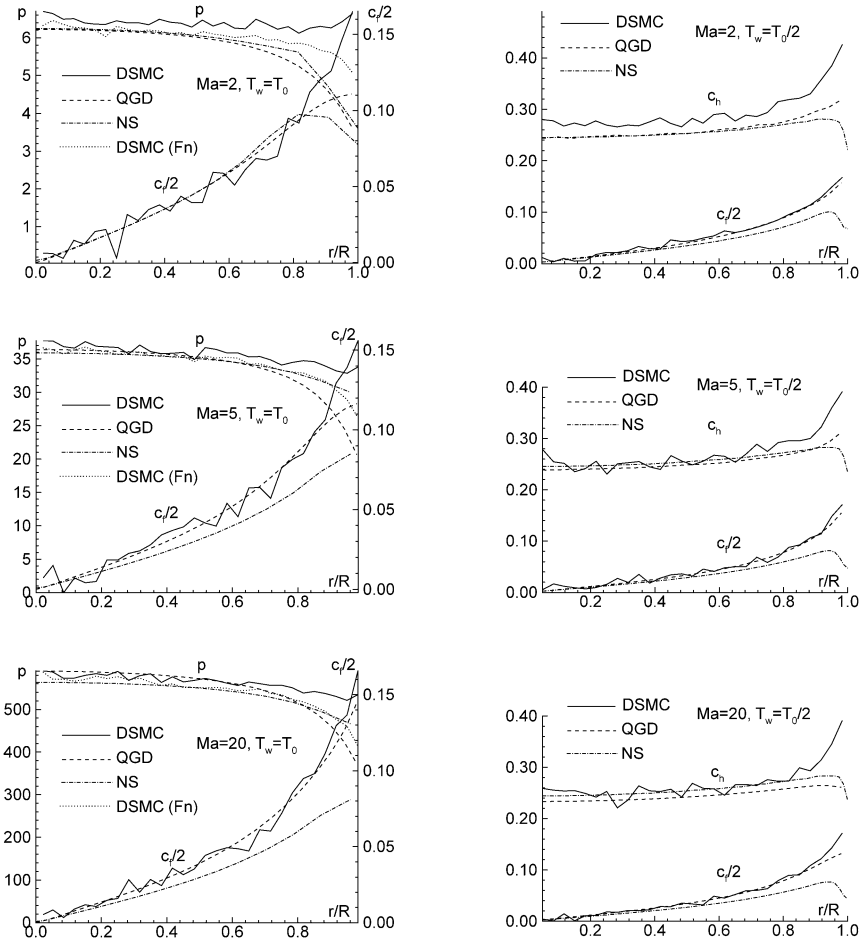

Fig. 3. Wall quantities: $T_w = T_0$ (left), $T_w = T_0/2$ (right).

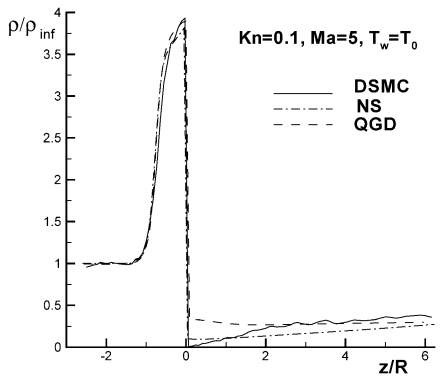

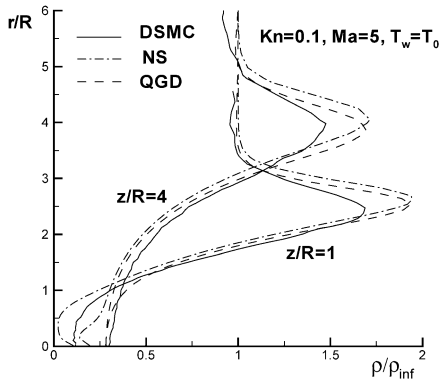

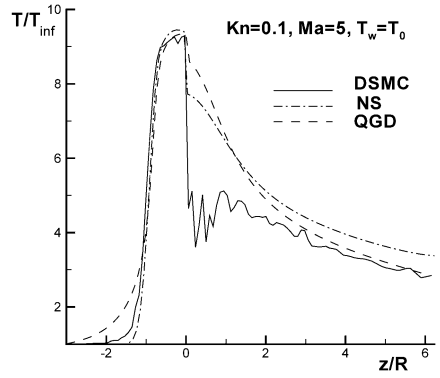

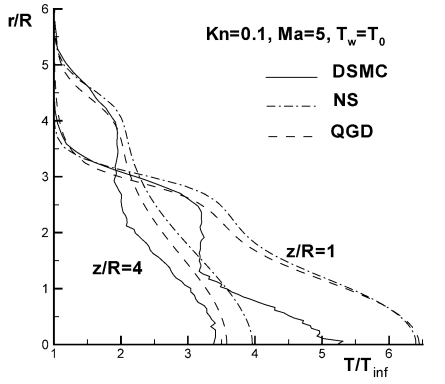

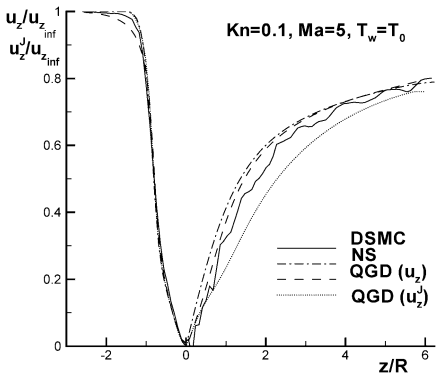

Fig. 4. Axial profiles of ρ (a), T (b) and u_z (c) ($Ma_\infty = 5$, $T_w = T_0$).

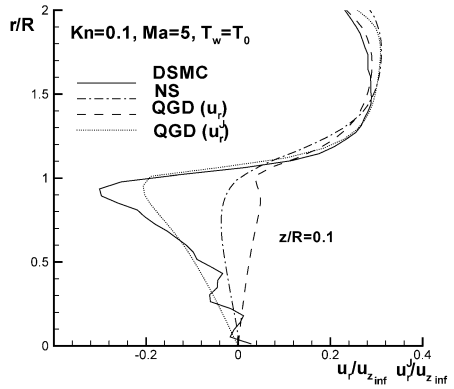

Fig. 5. Transverse profiles of ρ (a), T (b) and u_r (c) ($Ma_\infty = 5$, $T_w = T_0$).

the methods are observed in the near wake, where continuum approaches result in much higher densities and temperatures, QGD density and pressure being larger than NS ones. QGD temperature near the wall is closer to T_w than NS one (see Table 1), consistent with a smaller temperature jump. In this case $T_w = T_0 = 9.33\,T_\infty$. For the axial velocity distributions DSMC velocity is found between u_z and u_z^J, where u_z computed by NS and QGD models are rather similar. With increasing z, where τ and local Knudsen number become smaller, u_z^J and u_z computed by all three methods coincide. It is actually observed that the far wake tends to coincide for all three calculations.

Transverse profiles of density and temperature obtained by the three methods for $Ma_\infty = 5$, $T_w = T_0$ at $z/R = 1$ and 4 are presented in Fig. 5(a) and (b). NS and QGD profiles are quite close to one another. The main departure from DSMC is seen on the temperature distributions at $z/R = 1$. Transverse velocity profiles close to the disk surface ($z/R = 0.1$) are presented in

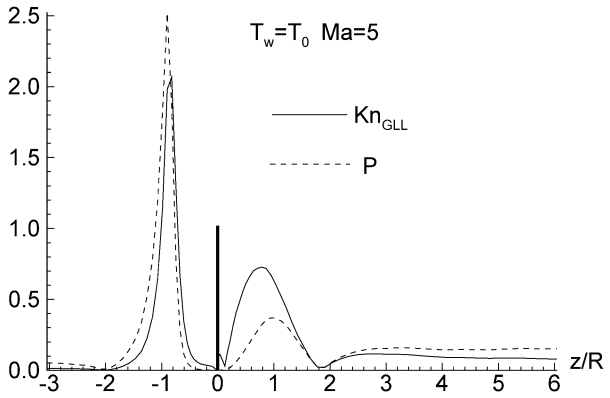

Fig. 6. Axial profiles of local Knudsen number and P parameter for QGD calculations ($Ma_\infty = 5$, $T_w = T_0$).

Fig. 5(c). Here the differences between the u_r^J and u_r velocities are significant because of the large local Knudsen numbers resulting in large values of τ. Here DSMC results correspond well with the QGD u_r^J velocity, but not with the u_r obtained by NS and QGD.

The density just behind the disk is very low. DSMC calculations indicate that $\rho/\rho_\infty \approx 0.05$ at $Ma_\infty = 2$ and is even smaller at $Ma = 5$ and 20. Thus the local mean free path is large ($20\lambda_\infty$, or $4R$ at $Ma_\infty = 2$ and even larger at $Ma_\infty = 5$ and 20). The near wake is entirely within the Knudsen layer where continuum methods are not claimed to be valid.

The discussion on the validity range of a continuum approach is based on the following considerations. A gas is in near equilibrium (and its velocity distribution function is close to a Maxwellian one) if the variation of a macroscopic parameter Q is small over the distance travelled by a molecule between two successive collisions.

In a locally subsonic flow, the thermal speed is larger than the macroscopic flow velocity and that distance is the mean free path $\lambda = \bar{c}\,\tau_c$, with $\bar{c} = \sqrt{(8\mathcal{R}T)/(\mathcal{M}\pi)}$. The corresponding criterion writes

$$Kn_{\mathrm{GLL}} = \lambda|\vec{\nabla}Q|/|Q| \ll 1, \tag{15}$$

where Kn_{GLL} is a "gradient-length local" Knudsen number.

In a locally supersonic flow, molecules travel essentially at the flow velocity $\vec{u}$ and the above criterion writes

$$P = |\vec{u}\cdot\vec{\nabla}Q|/|Q| = \sqrt{\pi}\,s\lambda|\vec{\nabla}Q|\,|\cos\theta|/(2|Q|) \ll 1, \tag{16}$$

where we have introduced the molecular speed ratio $s = u/\sqrt{2\mathcal{R}T/\mathcal{M}}$ and the angle θ between the flow velocity and the direction of the gradient.

A particular case of the latter criterion has been introduced by Bird [1] for expanding flows. Q was taken as the density and P was termed a "breakdown parameter".

A unique criterion can be deduced from (15) and (16) as

$$\lambda\frac{|\vec{\nabla}Q|}{|Q|}\max\left(1, \frac{\sqrt{\pi}}{2}s|\cos\theta|\right) \ll 1. \tag{17}$$

The variations of both parameters Kn_{GLL} and P along the z axis are plotted in Fig. 6 for $Ma_\infty = 5$, $T_w = T_0$, taking $Q = \rho$ obtained from the QGD flowfield. In the supersonic regions (well ahead of the disk and in the far wake) P exceeds Kn_{GLL}, but in the subsonic regions (in the shock layer and in the near wake) $P < Kn_{\mathrm{GLL}}$. It is clearly seen, that the significant differences between NS, QGD and the reference DSMC model correspond to regions with high P and Kn_{GLL} values.

Examples of 2D flowfields are presented in Fig. 7 for the flow parameters ρ and T. DSMC results are plotted as a reference in both the upper and lower parts of the figures. They appear as symmetrical isolines (full lines). In addition, NS and QGD results are plotted respectively in the upper and lower parts (dotted lines). The extent of the upstream and lateral disturbances induced by the disk in the freestream is very similar when obtained by the three methods. However already mentioned differences are observed in the wake region. The coincidence with DSMC results is obtained more rapidly when using QGD rather than NS equations.

Other calculations were carried out for freestream Mach numbers equal to 2 and 20 for both levels of the wall temperatures $T_w = T_0$ and $T_w = T_0/2$ (not plotted here). The density and the temperature gradients near the forward-facing wall in the "cold wall" case are significantly larger than in the near-adiabatic case. These calculations lead to similar observations.

QGD and NS computations were also carried out for smaller Knudsen numbers $Kn = 0.01$ ($Ma_\infty = 2$, 5, and 10) and $Kn = 0.005$ ($Ma_\infty = 2$ and 5) in the near-adiabatic case ($T_w = T_0$). Decreasing Kn and/or decreasing Ma_∞ is favorable to local

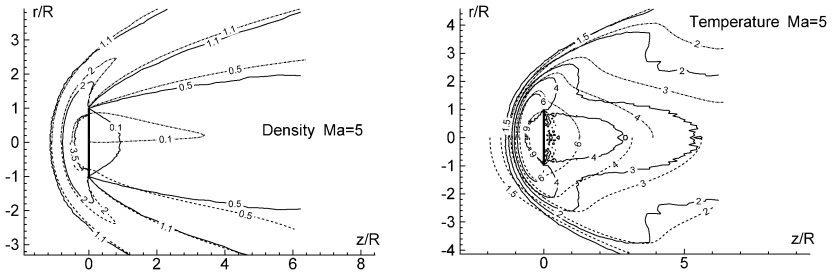

Fig. 7. 2D flowfields ($Ma_\infty = 5$, $T_w = T_0$). Left part: density. Right part: temperature. On both parts: DSMC (full lines). NS (long-dashed lines, upper half). QGD (dashed lines, lower half).

equilibrium and reduces the extent of the non-equilibrium region behind the disk. As a general conclusion, coming closer to local equilibrium makes QGD and NS results closer to one another.

8. Conclusion

The flow around a disk placed perpendicular to a supersonic rarefied flow has been calculated using NS and QGD equations. DSMC calculations have been used as a reference. All calculations were carried out with emphasis put on using correct criteria for time and space discretization.

A unique criterion for the validity of continuum equations has been presented. Usual criteria based on Knudsen number and Bird's breakdown parameter are particular cases of the present one, valid respectively for locally subsonic and locally supersonic regions of a flowfield.

Pressure and heat flux distributions along the forward-facing side of the disk depend little upon the model and are well described by both continuum NS and QGD equations for Knudsen numbers up to 0.1 and Mach numbers from 2 to 20.

QGD equations are clearly superior to NS ones for calculating the distribution of skin-friction in both the cold-wall and near-adiabatic cases. The QGD advantage increases with increasing the Mach number.

NS and QGD equations may be used for evaluating the flow parameters ahead of the disk up to Knudsen numbers equal to 0.1.

The near-wake region is within the Knudsen layer and cannot be described correctly by continuum approaches. Density and temperature levels behind the disk computed by NS and QGD models are large when compared with DSMC ones. However the radial velocity near the disk surface computed using the mass flux in QGD model is significantly closer to the DSMC results than the NS one. In the far wake QGD results coincide more rapidly with DSMC ones than do NS results.

Concerning the domain of validity of the QGD equations, the present work allows to conclude that, for the flows with small Knudsen numbers, where NS equations are valid, QGD additional dissipative terms do not distort the solution, but only stabilize the numerical algorithm.

For the flows with moderate Knudsen numbers, where the NS solution already departs from the DSMC one, it was expected that the QGD equations would bring some improvement to the NS solution, pushing it closer to the DSMC one. As demonstrated by the present work, this is true for a number of flow quantities or wall quantities. However for a few other quantities (e.g. flow temperature) QGD results exhibit no improvement (or even a degradation), compared with NS ones.

References

[1] G.A. Bird, Molecular Gas Dynamics and the Direct Simulation of Gas Flows, Clarendon Press, Oxford, 1994.
[2] T.G. Elizarova, Yu.V. Sheretov, Theoretical and numerical investigation of quasigasdynamic and quasihydrodynamic equations, Comput. Math. Math. Phys. 41 (2001) 219–234.
[3] T.G. Elizarova, I.A. Graur, J.C. Lengrand, A. Chpoun, Rarefied gas flow simulation based on quasi-gas dynamic equations, AIAA J. 33 (1995) 2316–2324.
[4] T.G. Elizarova, Yu.V. Sheretov, Analyse du problème de l'écoulement gazeux dans les microcanaux par les équations quasi hydrodynamiques, La Houille Blanche, No. 5, 2003, pp. 66–72.
[5] B. Mate, I.A. Graur, T.G. Elizarova, I.A. Chirokov, G. Tejeda, J.M. Fernandez, S. Montero, Experimental and numerical investigation of an axisymmetric supersonic jet, J. Fluid Mech. 426 (2001) 177–197.
[6] I.A. Graur, T.G. Elizarova, A. Ramos, G. Tejeda, J.M. Fernandez, S. Montero, A Study of shock waves in expanding flows on the basis of spectroscopic experiments and quasi-gasdynamic equations, J. Fluid Mech. 504 (2004) 239–270.

[7] T.G. Elizarova, I.A. Graur, J.C. Lengrand, Two-fluid computational model for a binary gas mixture, Eur. J. Mech. B Fluids 20 (2001) 351–369.
[8] J.N. Moss, V.K. Dogra, R.G. Wilmoth, DSMC simulations of Mach 20 nitrogen flows about 70° blunted cone and its wake, NASA TM 107762, 1993.
[9] E. Chabut, J.C. Lengrand, Simulation of a hypersonic flow during a Mars entry, in: Proc. of the 3th Intern. Symp. Atmospheric Reentry Vehicles and Systems, Association Aéronautique et Astronautique de France (AAAF), 2003, CD-ROM to be published.
[10] AMTEC Eng. Inc. INCA user's manual, Bellevue, 1992, WA 98009-3633.